Strong metal support interaction in Ru/V_2O_3 catalyst reduces reactant induced poisoning during succinic acid hydrogenation

Yayati Naresh Palai, [†] *Eti Mahal,* [‡] *Biswarup Pathak,* [‡*] *Atsushi Fukuoka* [†*], *Abhijit Shrotri*[†*]

[†] Institute for Catalysis, Hokkaido University, Sapporo, Hokkaido, Japan, 001-0021

[‡]Department of Chemistry, Indian Institute of Technology (IIT) Indore, Indore, Madhya Pradesh, India, 453552

Email: ashrotri@cat.hokudai.ac.jp

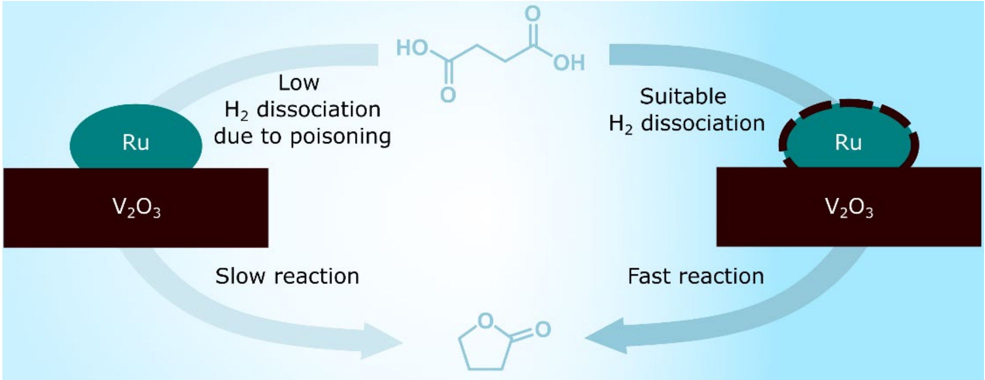

Keywords: Strong metal support interaction, V_2O_3 support, succinic acid hydrogenation, hydrogen spillover, gamma-butyrolactone

Abstract

Hydrogenation of carboxylic acids to lactones and alcohols is an important reaction. However, strong adsorption of carboxylic acid on the catalyst surface leads to poisoning of the active site, demands harsher reaction condition and use of organic solvents. In this study, we demonstrate that the strong metal support interaction (SMSI) and hydrogen spillover on Ru/V_2O_3 can counter the poisoning effect. The Ru/V_2O_3 catalysts reduced at 400 °C formed a layer of V_2O_3 over Ru. The catalyst was able to hydrogenate succinic acid to γ-butyrolactone (GBL) in 77 % yield in the presence of water at mild conditions of 150 °C and 6 h. H_2-D_2 exchange experiment showed that for the Ru/V_2O_3 without SMSI the H_2 dissociation was inhibited due to the adsorption of substrate over Ru surface, whereas catalysts with SMSI effect created a barrier between the substrate and the hydrogen dissociation sites. Spillover of dissociated H_2 onto the V_2O_3 surface was found to enhance the catalytic activity. Thermodynamics calculations using density functional theory showed that transfer of a hydride from Ru and proton from V_2O_3 to the substrate have a lower reaction free energy compared to that of transfer of two hydrogen atoms from a bare ruthenium surface. Additionally, weaker adsorption of substrates and easier desorption of product from the Ru/V_2O_3 surface increased catalytic activity compared to that of bare ruthenium surface. We show that the general concept of using SMSI to mitigate poisoning can be applied to catalytic hydrogenation of substrates that adsorb on metal sites.

1. Introduction

Hydrogenation of carboxylic acids to alcohols and lactones is an important reaction in biomass chemistry. Biobased diacids like succinic acid can be hydrogenated to produce γ-butyrolactone (GBL) [1–6], 1,4-butanediol (BDO) [7,8], and tetrahydrofuran (THF) [9–13] and used as alternative to petroleum [14]. Succinic acid hydrogenation to GBL (**Fig.** 1) is attractive because GBL is a useful solvent and intermediate to other biobased chemicals [15–18]. Supported Pt, Pd, Rh, Ru catalysts have been reported for hydrogenation of succinic acid to GBL typically at 240 °C, 6 MPa or higher H_2 pressure using 1,4-dioxane as solvent [1–6]. While several of these studies report good yield of GBL, it is necessary to design catalysts that operate at mild condition in the presence of water to reduce the carbon footprint of the process.

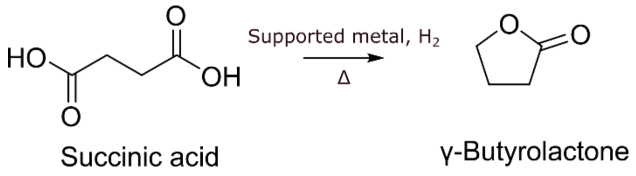

Fig. 1. Scheme showing succinic acid hydrogenation to GBL.

Use of oxophilic metals to enhance adsorption of intermediates [8,9], size reduction of metals to enhance atom utilization efficiency [4], and tuning of acidity/basicity of supports [5] are some of the strategies to design catalysts for succinic acid hydrogenation. However, reports on identifying the sites for adsorption of carboxylic acid and their influence on catalytic activity are less studied. Carboxylic acids are known to strongly adsorb on metal surfaces, which poisons the active sites and reduces activity at mild conditions [19–22]. Yakabi et al. reported that a strong bidentate adsorption of succinic acid over Ru lowers the selectivity of GBL due to decarboxylation, while monodentate adsorption on Pd showed higher selectivity of GBL [3]. Primo et al. reported that activity for hydrogenation of carboxylic acid can be increased using a Ru/TiO_2 where the carboxylic acid was weakly bound to the support near smaller metal nanoparticles, which provide H_2 for the hydrogenation reaction. In contrast, strongly bound carboxylic acid on Ru/CeO_2 was difficult to hydrogenate due to poisoning [23]. Additionally, strong coordination of dicarboxylic acids with metal atoms of catalyst also causes deactivation by leaching [19,20]. Therefore, limiting the strong adsorption of dicaboxylic acids on the metal surface should mitigate the poisoning of the active site and increase activity at mild conditions.

In this study, we show that by covering metal nanoparticle with oxide phase in Ru/V_2O_3 through strong metal support interaction (SMSI) [24–26], the substrate induced poisoning can be reduced by isolation of Ru sites from succinic acid. H_2 dissociation at the interface of Ru and V_2O_3 is enhanced in catalysts with SMSI. Furthermore, spillover of dissociated H_2 over the partially reduced V_2O_3 surface led to hydrogenation of succinic acid adsorbed on the support to GBL under mild reaction conditions in the presence of water.

2. Experimental

2.1 Catalyst synthesis

All the catalysts were prepared via wet impregnation method. In a typical synthesis, 500 mg of commercial V_2O_3 support (TCI Chemicals) was dispersed in 20 mL water, followed by addition of aqueous solution of $Ru(NO)(NO_3)_3$ to achieve 2 wt. % of ruthenium loading. The solution was evaporated at 40 °C at 60 mbar pressure, then the catalyst was dried and reduced at different temperatures for 1 h under 30 mL min^{-1} H_2 flow. The catalysts were named Ru/V_2O_3-X, where X was the reduction temperature. Catalysts using other supports was also prepared using the same method unless specified otherwise and reduced at 400 °C. The heating rate during reduction was set at 10 °C min^{-1} for all catalysts.

2.2 Catalyst characterization

X-ray diffraction (XRD) patterns were recorded with Rigaku Ultima IV using Cu Kα X-ray source (λ = 1.54 Å) operating at 40 kV and 20 mA. Scanning transmission electron microscopy (STEM) images were obtained in a JEOL JEM-ARM200F atomic resolution electron microscope. High resolution transmission electron microscopy (HR-TEM) images were taken on a JEOL JEM-2100F microscope. X-ray photoelectron spectroscopy (XPS) was performed with JEOL JPS-9010MC instrument with Mg anode. The spectra were charge corrected by adjusting the adventitious carbon peak to 284.6 eV. In-situ Fourier transformation infrared (FTIR) spectroscopy was carried out in Perkin Elmer Spectrum 100 IR instrument with a transmission cell (Schematic illustration in **Fig.** S1) and triglycerin sulphate (TGS) detector.

2.3 Succinic acid hydrogenation reaction

Succinic acid hydrogenation was performed in a 10 mL stainless steel autoclave reactor equipped with a teflon liner. In a typical reaction, 1 mmol of succinic acid and 50 mg of catalyst was added to 5 mL water. The reactor was closed and filled with 5 MPa of H_2 gas and placed in an oil bath preheated to 150 °C and was stirred through the entire course of reaction.

After the reaction, the reactor was cooled to room temperature and pressure was released. The recovered reaction mixture was centrifuged to separate the product mixture, which was analyzed with an HPLC equipped with an Aminex HPX 87H column and a RID detector with 0.5 mL/min flow of 5 mM H_2SO_4

solution at 50 °C. Succinic acid conversion (χ_t) and product yield (Y_p^t) at time, t was calculated using following equations –

$$\chi_t = \frac{n_r^0 - n_r^t}{n_r^0}$$

$$Y_p^t = \frac{n_p^t}{n_r^0}$$

Where n_r^0 and n_r^t are number of moles of reactant at time 0 and time t respectively and n_p^t is number of moles of product at time t.

2.4 Density Functional Theory Calculation

Theoretical calculations were performed with the help of Vienna *Ab initio* Simulation Package (VASP) [27,28]. The projected augmented wave method was implemented to describe the electron-core interactions with a plane wave basis set energy cutoff of 470 eV [29,30]. We have used the generalized gradient approximation as formulated in Perdew−Burke−Ernzerhof (GGA-PBE) functional to consider the exchange and correlation interaction [31]. DFT-D3 dispersion correction as implemented by Grimme was used [32]. We have utilized DFT+U approach proposed by Dudarev with U= 1.7 eV for V_2O_3, where the U value was chosen based on the previous theoretical studies on similar systems [33–35]. All the calculations performed were spin-polarized. Ru (001) slab was modelled with a (6×6) super cell having 4 layers. To design the Ru/V_2O_3 catalyst surface with SMSI, we have deposited one V_2O_3 (001) monolayer on top layer of the modelled Ru (001) slab as it is found to be the most stable surface of V_2O_3 in the previous studies [36]. A Γ-centered k-point mesh of 3×3×1 was used to sample the Brillouin zone. To avoid periodic interactions a vacuum of ~ 15 Å was added along the z-direction. The reaction free energy changes have been calculated using the following equation,

$$\Delta G = \Delta E + \Delta ZPE - T\Delta S$$

where ΔE is the total energy difference between initial and final states, ΔZPE is the change in zero-point energy. T and ΔS denotes temperature and change in entropy for the reaction, respectively. The 300 K temperature has been considered for the entropy correction and zero-point energy can be calculated considering the following equation,

$$ZPE = \sum_i {}^{1}/_{2}\, h\nu_i$$

Where ν_i and h are the vibrational frequencies and Planck's constant, respectively.

3. Results and Discussion

3.1 Characterization of Ru/V_2O_3 catalysts

Supported Ru/V_2O_3 catalysts were prepared for hydrogenation of succinic acid by impregnation with Ru loading of 2 wt. %. The catalysts were reduced at different temperatures to achieve varying degrees of SMSI. **Fig.** 2 shows XRD profiles of the Ru/V_2O_3 catalysts prepared by reducing Ru(NO)$(NO_3)_3$ impregnated V_2O_3 catalysts between 200 – 500 °C. All the catalysts showed peaks corresponding to V_2O_3 phase and no other phases of vanadium oxide were detected. The crystallite size of V_2O_3 was about 50 nm and did not change with an increase in reduction temperature. Ru crystallite size was beyond the detection limit of XRD as peaks corresponding to Ru nanoparticles were not observed in XRD pattern.

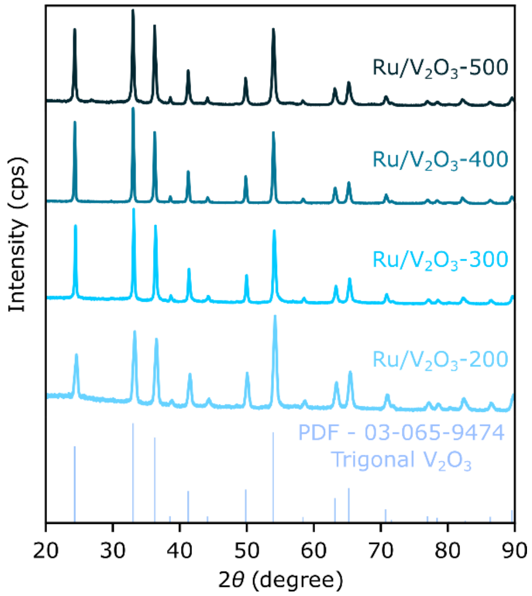

Fig. 2. XRD of Ru/V_2O_3 catalysts reduced at different temperatures along with standard trigonal V_2O_3 from PDF2 database.

Fig. 3a-h shows STEM images and corresponding particle size distribution of the Ru/V_2O_3 catalysts reduced at different temperatures. Most of the particles remained between 1.5 to 2 nm going from 200 °C to 400 °C as reduction temperature. However, in Ru/V_2O_3-500 a wider distribution was observed with few larger particles making the average particle size 2.8 nm. The surface area of the catalysts, calculated from N_2 adsorption isotherms, varied between 5.6–4.7 m^2g^{-1} (**Fig.** S2, Table S1). Therefore, despite the low surface area and high reduction temperature aggregation of Ru nanoparticles was limited.

All the catalysts showed a hazy amorphous phase around the particles, which suggests migration of V_2O_3 support over the surface of metal nanoparticles during the thermal reduction. **Fig.** 3i and **Fig.** 3j show the HR–TEM images of Ru/V_2O_3-400 and Ru/V_2O_3-500, respectively, having encapsulating layers of V_2O_3 confirming the occurrence of SMSI.

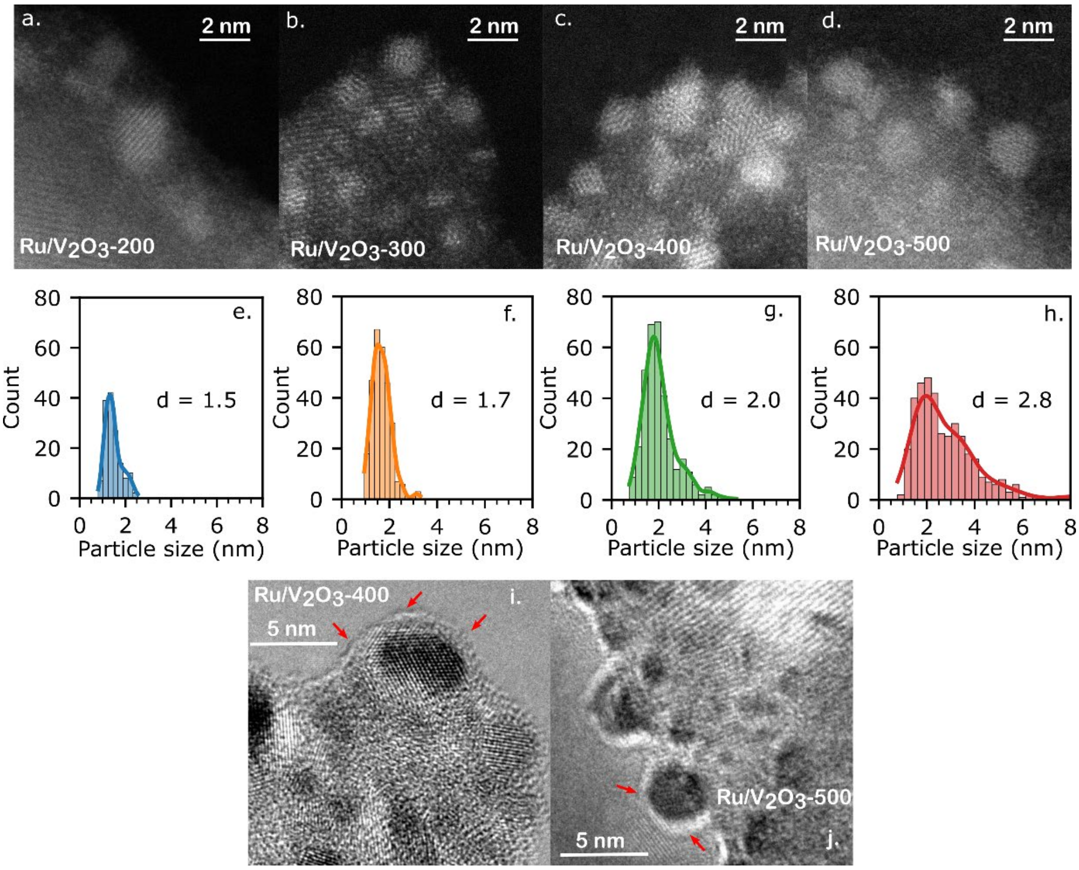

Fig. 3. (a-d) STEM images of Ru/V_2O_3 catalysts reduced at different temperatures. (e-h) Particle size distribution of Ru/V_2O_3 at different reduction temperatures. (i, j) HR-TEM images of Ru/V_2O_3-400 and Ru/V_2O_3-500.

Fig. 4a shows XPS of freshly reduced Ru/V_2O_3 catalysts at different temperatures. For all the catalysts an asymmetric photoemission signal centered at 280.0 eV was observed, which was assigned to Ru 3d 5/2 emission [37], and was fitted with two component peaks. The major component at 280.0 eV was assigned to metallic ruthenium species and the minor component at 280.7 eV was assigned to oxidized $Ru^{\delta+}$ species. The presence of $Ru^{\delta+}$ species was attributed to Ru atoms at the interface with V_2O_3 [38]. The percentage of metallic Ru increased with reduction temperature from 76 % for Ru/V_2O_3-200 °C to 91 % at Ru/V_2O_3-500 °C (**Fig.** S3). The increase in metallic component could be ascribed to increase in Ru nanoparticle size or to charge transfer from support to metal as the degree of SMSI progresses at higher temperature. In the O 1s region, two peaks centered at 530.0 eV and 531.6 eV were observed, which were assigned to the lattice oxygen of V_2O_3 and surface hydroxyl groups, respectively. The abundance of surface hydroxyl groups reduced with increase in reduction temperature because of dehydroxylation of support. This was further confirmed by a decrease in ratio of surface oxygen to vanadium with the increase in reduction temperature (**Fig.** 4b). Despite loss of some surface oxygen species the oxidation state of vanadium was V^{3+} as observed in the V 2p 3/2 region of the spectrum showing a single component peak at 515.6 eV (**Fig.** 4a) [39].

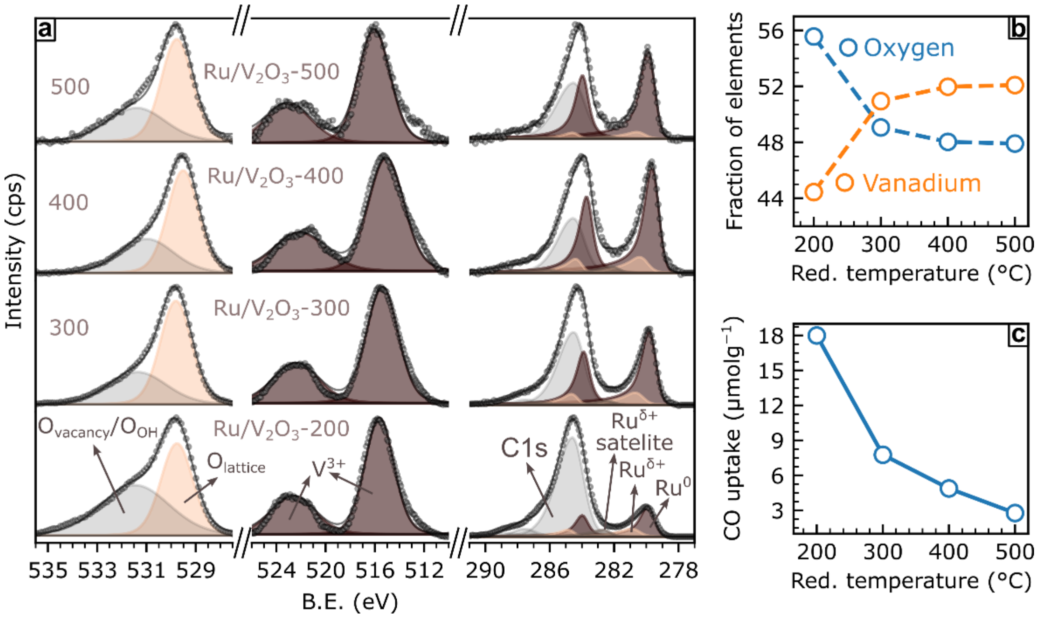

Fig. 4. (a) Deconvoluted O 1s, V 2p and Ru 3d 5/2 XPS of Ru/V_2O_3 reduced at different temperatures. (b) Variation of surface elemental composition as a function of reduction temperature. (c) CO chemisorption amount on Ru/V_2O_3 at different reduction temperatures.

Partial reduction of metal support interface is associated with the SMSI effect in supported metal oxides. Partial reduction lowers the work function causing charge transfer from support to metal nanoparticle and encapsulation of the metal nanoparticle [40]. **Fig.** 4c. shows that CO chemisorption amount decreased with the increase in reduction temperature, which corroborates with loss of chemisorption sites due to encapsulation of Ru nanoparticle by V_2O_3 layer as SMSI progresses.

3.2 Succinic acid hydrogenation

Fig. 5a shows the result of succinic acid hydrogenation at 150 °C in water in the presence of Ru/V_2O_3 catalysts as a function of the reduction temperature. In all cases GBL was the major product with small amounts of BDO, THF, butanol (BuOH) and propionic acid (PA). GBL yield increased with an increase in reduction temperature up to 400 °C. Further increase in the reduction temperature to 500 °C decreased the catalytic activity for succinic acid hydrogenation as the degree of SMSI and Ru particle size increased.

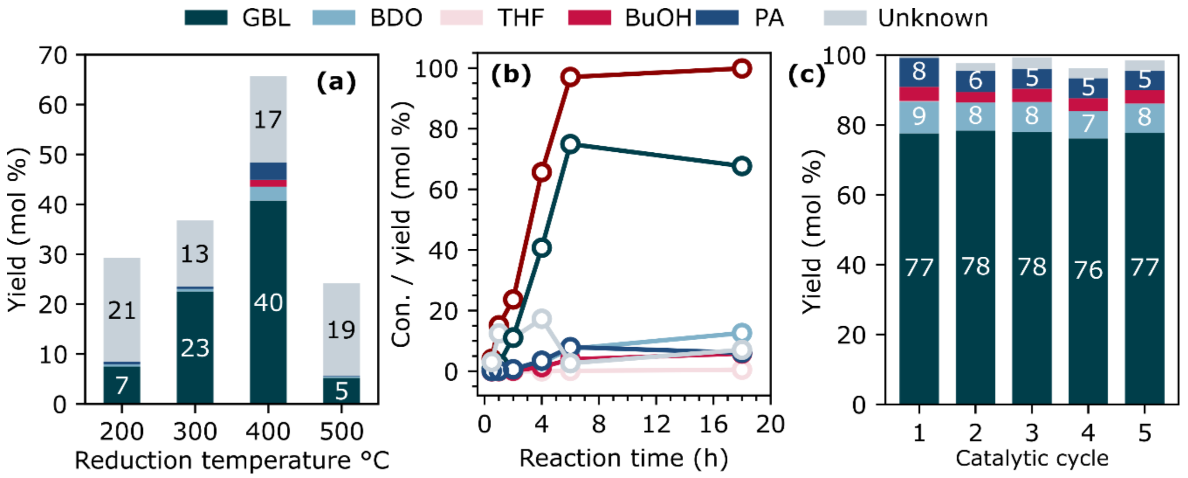

Fig. 5. (a) Activity of Ru/V_2O_3 catalysts as a function of reduction temperature, reaction conditions – succinic acid 0.118 g (1 mmol), catalyst 0.05 g, water 5 mL, H_2 5 MPa, 150 °C, 4 h. (b) Succinic acid hydrogen reaction time course, reaction conditions – succinic acid 0.118 g (1 mmol), catalyst Ru/V_2O_3-400 (0.05g), H_2 5 MPa, 150 °C. (c) Catalyst recycling study of Ru/V_2O_3-400 at full conversion, reaction conditions – succinic acid 0.118 g (1 mmol), catalyst 0.05 g, H_2 5 MPa, 150 °C, 6 h.

Evolution of products over time was studied to understand the reaction pathway and optimal reaction time using Ru/V_2O_3-400 catalyst (**Fig.** 5b). Succinic acid was completely converted in 6 hours and GBL yield was 77%. Further continuing the reaction to 18 hours converted some of the GBL to BDO, which shows that GBL was stable under the reaction condition. The Ru/V_2O_3-400 catalyst was found to be recyclable for at least up to 5 cycles and there was no loss of activity during the recycling experiments (**Fig.** 5c).

3.3 Role of SMSI in minimization of substrate induced hydrogen dissociation.

Catalysts reduced at 200 °C showed low activity for succinic acid hydrogenation even though it contained highest number of exposed Ru particles as per CO chemisorption. To investigate the role of SMSI on catalytic activity we studied the hydrogen dissociation over the catalyst by H_2-D_2 exchange in the presence and absence of an adsorbate. A mixture of H_2-D_2 was flown over freshly reduced catalyst while measuring the HD intensity. The H-D exchange reaction was allowed to equilibrate at 50 °C for 15 minutes and then the temperature was increased to 150 °C at a rate of 10 °C/min. At 50 °C all catalysts except Ru/V_2O_3-200 showed similar HD intensity in the absence of any adsorbate (denoted as clean surface in **Fig.** 6 a-d). Because the degree of SMSI was higher as temperature increased, we propose that hydrogen spillover at the interface of Ru and V_2O_3, formed via SMSI, contributed towards the higher rate of H-D exchange. Increasing the temperature of H-D exchange experiment from 50 °C to 150 °C increased the HD intensity suggesting that thermodynamic equilibrium was not reached, and the H-D exchange reaction was within kinetic control regime.

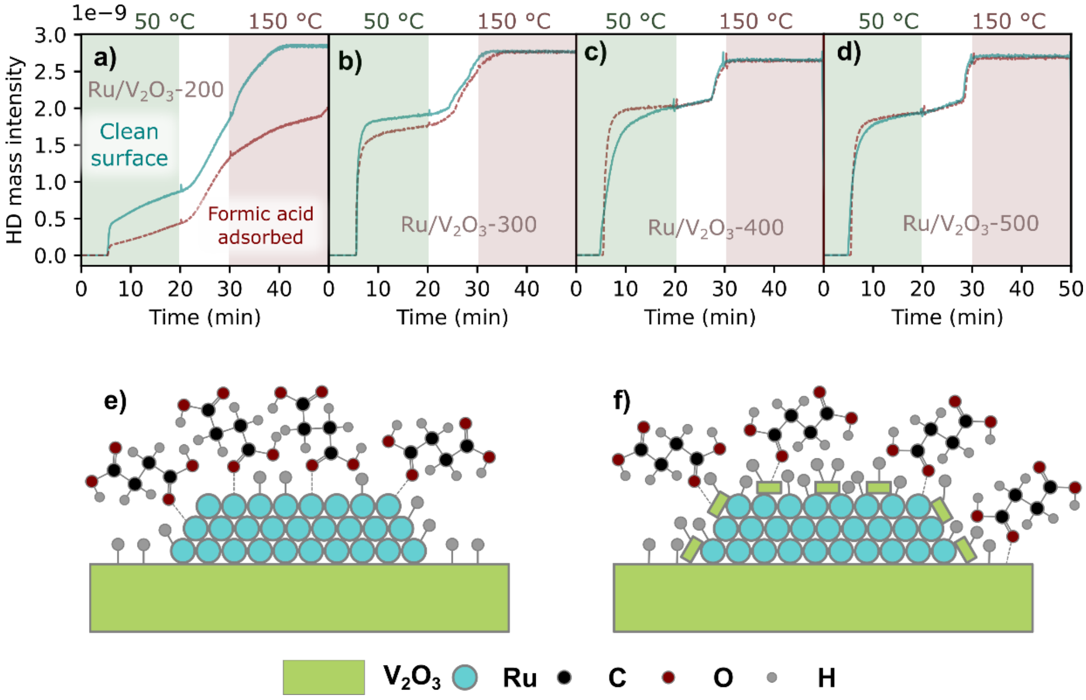

Fig. 6. (a-d) Mass intensity of HD in the presence of Ru/V_2O_3 catalysts in the absence and presence of formic acid on the surface. (e, f) Schematic representation of the effect of formic acid adsorption on the catalysts with and without SMSI.

Next, we adsorbed formic acid on the catalysts to test the H-D exchange ability in the presence of an adsorbate with carboxyl group. Formic acid was chosen over succinic acid as adsorbate because formic acid is volatile and can be deposited over the catalyst in-situ after reduction. The HD intensity over Ru/V_2O_3-200 decreased further in the presence of formic acid, indicating that Ru surface without SMSI was poisoned by the adsorbate and the hydrogen dissociation ability reduced. However, with the increase in catalyst reduction temperature, the HD intensity for Ru/V_2O_3-400 in the presence of formic acid was similar to the HD intensity over clean surface. These results suggest that coverage of Ru surface by V_2O_3 mitigates the poisoning of the catalyst. In the SMSI catalyst the formic acid would adsorb over the V_2O_3 layer instead of Ru sites and would prevent the loss of hydrogen dissociation ability.

3.4 Hydrogen dissociation and spillover over interface of Ru/V_2O_3

Through the HD exchange experiment it was evident that the SMSI enhanced the H_2 dissociation ability in the presence of an adsorbate. In the catalyst with SMSI, hydrogenation of succinic acid adsorbed on the V_2O_3 layer would require spillover of H_2. The spillover was studied by analyzing the reduction of WO_3 in a physical mixture of Ru/V_2O_3 and WO_3. First, temperature programmed reduction (TPR) of Ru/V_2O_3 (**Fig.** 7a) was measured, which showed a broad reduction peak between 300 °C to 480 °C. In comparison, the TPR profile of Ru/SiO_2 (prepared as a control catalyst) was narrower and spanned from 200 °C to 300 °C, suggesting a stronger interaction between Ru and V_2O_3 compared to that of Ru and SiO_2. The significantly higher area and the asymmetric shape of the reduction peak in case of Ru/V_2O_3 suggests partial reduction of V_2O_3 support. Partial reduction of support is known to trigger the diffusion of support phase onto the metal nanoparticle in case of reducible oxides to cause SMSI [40].

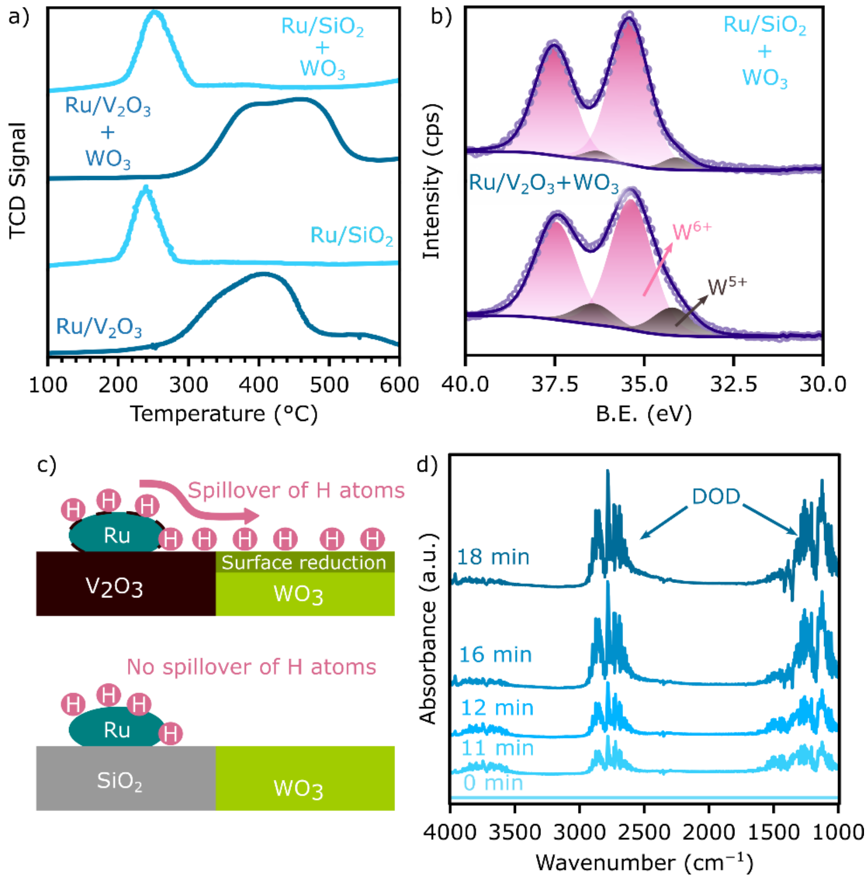

Fig. 7. (a) TPR profiles of Ru/V_2O_3 and Ru/SiO_2 and their physical mixture with WO_2. (b) W 4f XPS of physical mixtures of Ru/V_2O_3 and Ru/SiO_2 with WO_3 after the TPR experiment. (c) Scheme showing surface reduction of WO_3 in physical contact with Ru/V_2O_3 due to hydrogen spillover. (d) In-situ D_2 FTIR over Ru/V_2O_3 400 catalyst.

TPR profile of physical mixture of tungsten oxide and Ru/SiO_2 was similar to pure Ru/SiO_2 with a rising tail around 600 °C. Reduction of physically mixed tungsten oxide would require spillover of dissociated hydrogen to reduce WO_3 as shown in **Fig.** 7c. When the TPR experiment was conducted with physical mixture of WO_3 and Ru/V_2O_3 a new peak centered around 500 °C appeared, which was assigned to reduction of WO_3 via spillover of dissociated hydrogen. XPS of the physical mixture after the TPR experiment showed presence of significant amount of W^{5+} (**Fig.** 7b), which confirmed the ease of hydrogen spillover over V_2O_3.

Hydrogen spillover involves either the migration of a hydrogen atom or a proton from the metal to support. While the electrons would enter the conduction band of the support, the protons would bond to the surface oxygen species. In absence of reactants, the formed OH groups would eventually lead to formation of either surface or gas phase water molecules, which was monitored by in-situ IR spectroscopy. When D_2 was flown through the sample reduced in-situ at 400 °C, there was a gradual increase in signal around 2500 to 3000 cm^{-1} region and 1300 to 1000 cm^{-1} as shown in **Fig.** 7d. The former was attributed to OD stretching frequency and the latter to OD bending frequency [45–47]. The OD formation on oxide supports could also occur via exchange of D with support hydroxyl protons. However, loss of hydroxyl protons in such a manner must be accompanied by development of negative peak around OH region in the IR spectrum, which was not observed. Hence, the formation of OD could be assigned to the spilled over D^+ ions indicating formation of a proton-hydride pair and spillover mechanism for Ru/V_2O_3 catalysts with SMSI.

3.5 DFT calculation to show hydrogen heterolysis is more efficient in succinic acid hydrogenation

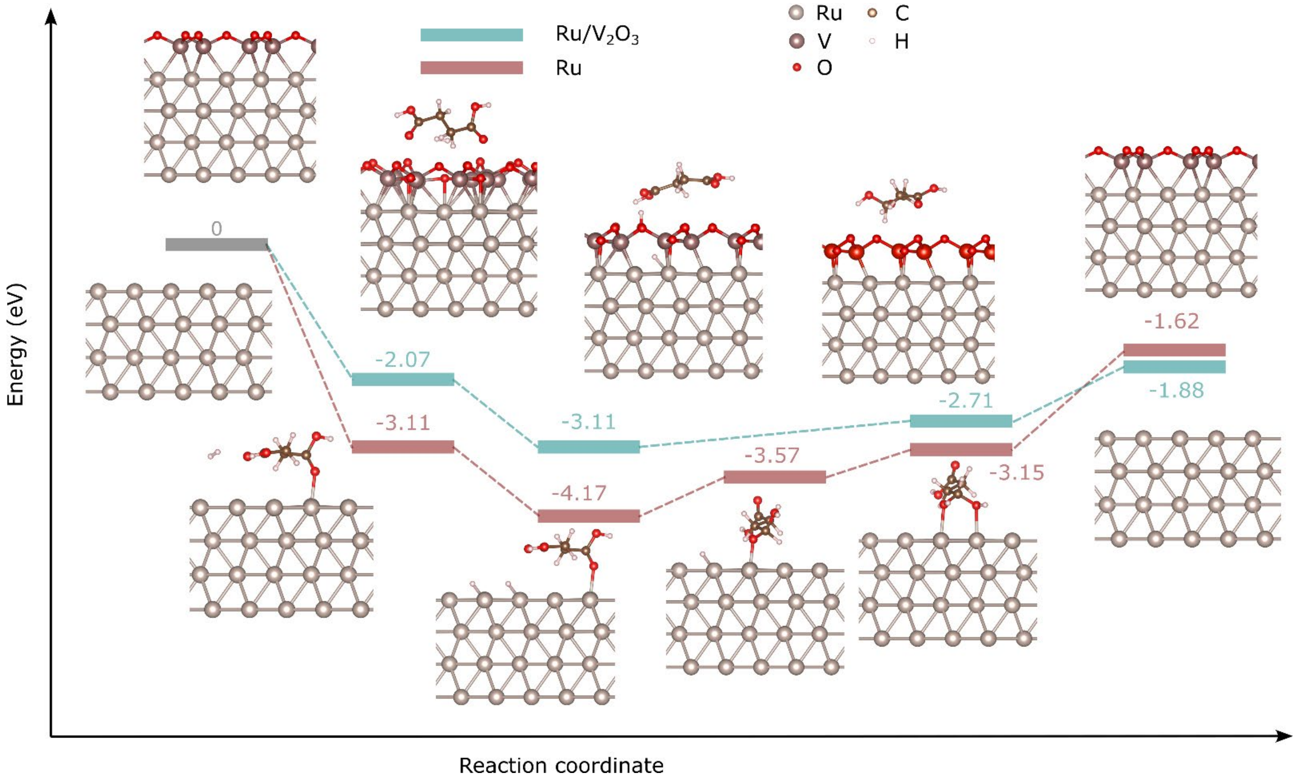

Fig. 8. Reaction free energy (in eV) profile of various intermediates in the succinic acid hydrogenation over bare ruthenium surface and Ru/V_2O_3 surface.

Experimental observations of SMSI and its effect in enhancing hydrogenation of succinic acid were also evaluated by theoretical calculation. The Ru/V_2O_3 catalyst with SMSI was modelled considering a monolayer of V_2O_3 deposited on Ru (001) and it was compared with bare Ru (001) as a model for catalyst without SMSI (**Fig.** 8, and **Fig.** S4-S6). Calculation results showed that homolytic dissociation of H_2 was preferred over bare Ru (001) surface. In contrast, H_2 underwent heterolytic cleavage on the Ru/V_2O_3 surface. The heterolytic cleavage on Ru/V_2O_3 was possible due to the presence of electron rich O of V_2O_3 layer and the electron deficient Ru, which attracted the proton and the hydride, respectively. Upon introduction of succinic acid, a sequential hydrogenation pathway was observed on the bare Ru (001). Consecutive transfer of dissociated H occurred from the bare Ru (001) surface to the carbonyl carbon and oxygen atom of succinic acid. The overall change in reaction free energy (**Fig.** 8) for the consecutive steps was 1.02 eV (-4.17 eV to -3.15 eV). However, for the Ru/V_2O_3, hydrogenation with proton and hydride in a concerted mechanism was more favored. The change in reaction free energy was 0.40 eV (-3.11 eV to -2.71 eV), which was less than that for bare Ru(001) without SMSI. In addition, the desorption free energy of the product from the Ru/V_2O_3 surface was 0.83 eV (-2.71 eV to -1.88 eV). In comparison, the desorption free energy of product from bare Ru(001) surface was higher at 1.53 eV (-3.15 eV to -1.62 eV). Therefore, the calculation results show that succinic acid hydrogenation through heterolytic dissociation of H_2, desorption of product and regeneration of the active site would be facile on the Ru/V_2O_3 catalyst surface with SMSI, which aligns with the experimental outcomes.

3.6 Conclusion

In conclusion, SMSI effect along with hydrogen spillover in Ru/V_2O_3 could lead to effective hydrogenation of succinic acid at mild condition by reducing substrate induced poisoning of hydrogen dissociation sites. STEM and TEM images along with XPS and CO pulse chemisorption confirmed the occurrence of SMSI effect in Ru/V_2O_3 catalysts reduced at higher temperature. Catalyst reduced at 400 °C with optimal SMSI degree produced GBL yield of 77% at mild condition of 150 °C and in the presence of water. Decrease in HD formation from $H_2 – D_2$ exchange reaction in presence of adsorbed formic acid illustrated poisoning of hydrogen dissociation sites in catalysts without SMSI. In-situ D_2 IR confirmed formation of proton-hydride species on V_2O_3 surface owing to heterolytic dissociation. According to density functional theory calculations, easier hydrogenation and facile desorption of product from the Ru/V_2O_3 surface in SMSI state makes it a better catalyst for the process compared to clean ruthenium surface.

CRediT authorship contribution statement

Yayati Naresh Palai: Conceptualization; Data curation; Formal analysis; Investigation; Methodology; Visualization; Writing - original draft; and Writing - review & editing

Eti Mahal: Data curation; Investigation; Writing - original draft

Biswarup Pathak: Resources; Supervision; Writing - review & editing

Abhijit Shrotri: Conceptualization; Project administration; Supervision; Resources; Validation; Writing - review & editing

Atsushi Fukuoka: Funding acquisition; Resources; Writing - review & editing

Declaration of Competing Interest

The authors declare that they have no known competing financial interests or personal relationships that could have appeared to influence the work reported in this paper.

Data availability

Data will be made available on request.

Acknowledgements

Part of this research was supported by JACI Prize for Encouraging Young Researcher and Hokkaido University Creative Young Researcher Acceleration Project. A part of this work was supported by "Advanced Research Infrastructure for Materials and Nanotechnology in Japan (ARIM)" of the Ministry of Education, Culture, Sports, Science and Technology (MEXT), proposal number JPMXP1223HK0088. Also, we thank IIT Indore for the computing facilities. Part of this work is supported by DST-SERB (Project Number CRG/2022/000836), CSIR (Project Number 01(3046)/21/EMR-II), and BRNS (Project Number 2023-BRNS/12356). E.M. thanks MoE for research fellowship.

References

[1] G. Budroni, A. Corma, Gold and gold–platinum as active and selective catalyst for biomass conversion: Synthesis of γ-butyrolactone and one-pot synthesis of pyrrolidone, Journal Of Catalysis 257 (2008) 403–408. https://doi.org/10.1016/j.jcat.2008.05.031.

[2] U.G. Hong, S. Hwang, J.G. Seo, J. Lee, I.K. Song, Hydrogenation of succinic acid to γ-butyrolactone (GBL) over palladium catalyst supported on alumina xerogel: Effect of acid density of the catalyst, Journal Of Industrial Engineering Chemistry 17 (2011) 316–320. https://doi.org/10.1016/j.jiec.2011.02.030.

[3] K. Yakabi, A. Jones, A. Buchard, A. Roldan, C. Hammond, Chemoselective lactonization of renewable succinic acid with heterogeneous nanoparticle catalysts, ACS Sustainable Chemistry Engineering 6 (2018) 16341–16351.

[4] C. Zhang, L. Chen, H. Cheng, X. Zhu, Z. Qi, Atomically dispersed Pd catalysts for the selective hydrogenation of succinic acid to γ-butyrolactone, Catalysis Today 276 (2016) 55–61. https://doi.org/10.1016/j.cattod.2016.01.028.

[5] C. You, C. Zhang, L. Chen, Zhiwen. Qi, Highly dispersed palladium nanoclusters incorporated in amino-functionalized silica spheres for the selective hydrogenation of succinic acid to γ-butyrolactone., Applied Organometallic Chemistry 29 (2015) 653–660. https://doi.org/10.1002/aoc.3342.

[6] B. Tapin, F. Epron, C. Especel, B.K. Ly, C. Pinel, M. Besson, Study of Monometallic Pd/TiO_2 Catalysts for the Hydrogenation of Succinic Acid in Aqueous Phase, ACS Catalysis 3 (2013) 2327–2335. https://doi.org/10.1021/cs400534x.

[7] D.P. Minh, M. Besson, C. Pinel, P. Fuertes, C. Petitjean, Aqueous-Phase Hydrogenation of Biomass-Based Succinic Acid to 1,4-Butanediol Over Supported Bimetallic Catalysts, Topics In Catalysis 53 (2010) 1270–1273. https://doi.org/10.1007/s11244-010-9580-y.

[8] K.H. Kang, U.G. Hong, Y. Bang, J.H. Choi, J.K. Kim, J.K. Lee, S.J. Han, I.K. Song, Hydrogenation of succinic acid to 1,4-butanediol over Re–Ru bimetallic catalysts supported on mesoporous carbon, Applied Catalysis A General 490 (2015) 153–162. https://doi.org/10.1016/j.apcata.2014.11.029.

[9] S.D. Le, S. Nishimura, Effect of support on the formation of CuPd alloy nanoparticles for the hydrogenation of succinic acid, Applied Catalysis B Environmental 282 (2021) 119619. https://doi.org/10.1016/j.apcatb.2020.119619.

[10] Z. Shao, C. Li, X. Di, Z. Xiao, Changhai. Liang, Aqueous-Phase Hydrogenation of Succinic Acid to γ-Butyrolactone and Tetrahydrofuran over Pd/C, Re/C, and Pd-Re/C Catalysts., Industrial Engineering Chemistry Research 53 (2014) 9638–9645. https://doi.org/10.1021/ie5006405.

[11] X. Di, C. Li, B. Zhang, J. Qi, W. Li, D. Su, C. Liang, Role of Re and Ru in Re–Ru/C Bimetallic Catalysts for the Aqueous Hydrogenation of Succinic Acid, Industrial Engineering Chemistry Research 56 (2017) 4672–4683. https://doi.org/10.1021/acs.iecr.6b04875.

[12] R.M. Deshpande, V.V. Buwa, C.V. Rode, R.V. Chaudhari, P.L. Mills, Tailoring of activity and selectivity using bimetallic catalyst in hydrogenation of succinic acid., Catalysis Communications 3 (2002) 269–274. https://doi.org/10.1016/S1566-7367(02)00119-X.

[13] X. Liu, X. Wang, G. Xu, Q. Liu, X. Mu, Haichao. Liu, Tuning the catalytic selectivity in biomass-derived succinic acid hydrogenation on FeOx-modified Pd catalysts., Journal Of Materials Chemistry A Materials For Energy Sustainability 3 (2015) 23560–23569. https://doi.org/10.1039/C5TA03843J.

[14] S. Oka, Studies on Lactone Formation in Vapor Phase. III. Mechanism of Lactone Formation from Diols, Bulletin Of Chemical Society Of Japan 35 (1962) 986–989. https://doi.org/10.1246/bcsj.35.986.

[15] H. Kim, S. Yang, D.H. Kim, One-pot conversion of alginic acid into furfural using Amberlyst-15 as a solid acid catalyst in γ-butyrolactone/water co-solvent system, Environmental Research 187 (2020) 109667. https://doi.org/10.1016/j.envres.2020.109667.

[16] L. Wang, H. Guo, Q. Xie, J. Wang, B. Hou, L. Jia, J. Cui, D. Li, Conversion of fructose into furfural or 5-hydroxymethylfurfural over HY zeolites selectively in Γ-butyrolactone, Applied Catalysis A General 572 (2019) 51–60. https://doi.org/10.1016/j.apcata.2018.12.023.

[17] J.H. Ter Horst, R.M. Geertman, G.M. Van Rosmalen, The effect of solvent on crystal morphology, Journal Of Crystal Growth 230 (2001) 277–284. https://doi.org/10.1016/S0022-0248(01)01341-0.

[18] W. Schwarz, J. Schossig, R. Rossbacher, R. Pinkos, H. Höke, Butyrolactone, in: Ullmanns Encyclopedia Of Industrial Chemistry, Wiley-VCH, Weinheim, 2019: pp. 1–7.

https://onlinelibrary.wiley.com/doi/full/10.1002/14356007.a04_495.pub2 (accessed September 17, 2021).

[19] L. Karam, C.N. Neumann, Heterogeneously Catalyzed Carboxylic Acid Hydrogenation to Alcohols, ChemCatChem 14 (2022) e202200953. https://doi.org/10.1002/cctc.202200953.

[20] Y. Takeda, M. Tamura, Y. Nakagawa, K. Okumura, K. Tomishige, Characterization of Re–Pd/SiO_2 Catalysts for Hydrogenation of Stearic Acid, ACS Catalysis 5 (2015) 7034–7047. https://doi.org/10.1021/acscatal.5b01054.

[21] M. Guo, X. Kong, C. Li, Q. Yang, Hydrogenation of benzoic acid derivatives over Pt/TiO_2 under mild conditions, Communications Chemistry 4 (2021) 1–10. https://doi.org/10.1038/s42004-021-00489-z.

[22] X. Cui, Y. Li, C. Topf, K. Junge, M. Beller, Direct Ruthenium-Catalyzed Hydrogenation of Carboxylic Acids to Alcohols, Angewandte Chemie International Edition 54 (2015) 10596–10599. https://doi.org/10.1002/anie.201503562.

[23] A. Primo, P. Concepción, A. Corma, Synergy between the metal nanoparticles and the support for the hydrogenation of functionalized carboxylic acids to diols on Ru/TiO_2, Chemical Communications 47 (2011) 3613–3615. https://doi.org/10.1039/c0cc05206j.

[24] S.J. Tauster, S.C. Fung, R.T.K. Baker, J.A. Horsley, Strong Interactions in Supported-Metal Catalysts, Science 211 (1981) 1121–1125. https://doi.org/10.1126/science.211.4487.1121.

[25] S.J. Tauster, S.C. Fung, R.L. Garten, Strong metal-support interactions. Group 8 noble metals supported on titanium dioxide, Journal Of American Chemical Society 100 (1978) 170–175. https://doi.org/10.1021/ja00469a029.

[26] S.J. Tauster, S.C. Fung, Strong metal-support interactions: Occurrence among the binary oxides of groups IIA–VB, Journal Of Catalysis 55 (1978) 29–35. https://doi.org/10.1016/0021-9517(78)90182-3.

[27] G. Kresse, J. Furthmüller, Efficient iterative schemes for ab initio total-energy calculations using a plane-wave basis set, Physical Review B 54 (1996) 11169. https://doi.org/10.1103/PhysRevB.54.11169.

[28] G. Kresse, J. Hafner, Ab initio molecular dynamics for liquid metals, Physical Review B 47 (1993) 558. https://doi.org/10.1103/PhysRevB.47.558.

[29] P.E. Blöchl, Projector augmented-wave method, Physical Review B 50 (1994) 17953–17979. https://doi.org/10.1103/PhysRevB.50.17953.

[30] G. Kresse, D. Joubert, From ultrasoft pseudopotentials to the projector augmented-wave method, Physical Review B 59 (1999) 1758–1775. https://doi.org/10.1103/PhysRevB.59.1758.

[31] J.P. Perdew, K. Burke, M. Ernzerhof, Generalized Gradient Approximation Made Simple, Physical Review Letters 77 (1996) 3865–3868. https://doi.org/10.1103/PhysRevLett.77.3865.

[32] S. Grimme, J. Antony, S. Ehrlich, H. Krieg, A consistent and accurate ab initio parametrization of density functional dispersion correction (DFT-D) for the 94 elements H-Pu, Journal Of Chemical Physics 132 (2010) 154104. https://doi.org/10.1063/1.3382344.

[33] V.I. Anisimov, F. Aryasetiawan, A.I. Lichtenstein, First-principles calculations of the electronic structure and spectra of strongly correlated systems: the LDA+ U method, Journal Of Physics Condensed Matter 9 (1997) 767. https://doi.org/10.1088/0953-8984/9/4/002.

[34] S.L. Dudarev, G.A. Botton, S.Y. Savrasov, C.J. Humphreys, A.P. Sutton, Electron-energy-loss spectra and the structural stability of nickel oxide: An LSDA+U study, Physical Review B 57 (1998) 1505–1509. https://doi.org/10.1103/PhysRevB.57.1505.

[35] J. Goniakowski, C. Noguera, Properties of M_2O_3/Au(111) Honeycomb Monolayers (M = Sc, Ti, V, Cr, Mn, Fe, Co, Ni), Journal Of Physical Chemistry C 123 (2019) 9272–9281. https://doi.org/10.1021/acs.jpcc.9b01429.

[36] G. Kresse, S. Surnev, J. Schoiswohl, F.P. Netzer, V2O3(0001) surface terminations: a density functional study, Surface Science 555 (2004) 118–134. https://doi.org/10.1016/j.susc.2004.02.009.

[37] D.J. Morgan, Resolving ruthenium: XPS studies of common ruthenium materials, Surface Interface Analysis 47 (2015) 1072–1079. https://doi.org/10.1002/sia.5852.

[38] J. Zhou, Z. Gao, G. Xiang, T. Zhai, Z. Liu, W. Zhao, X. Liang, L. Wang, Interfacial compatibility critically controls Ru/TiO2 metal-support interaction modes in CO2 hydrogenation, Nature Communications 13 (2022) 327. https://doi.org/10.1038/s41467-021-27910-4.

[39] G. Silversmit, D. Depla, H. Poelman, G.B. Marin, R. De Gryse, Determination of the V2p XPS binding energies for different vanadium oxidation states (V^{5+} to V^{0+}), Journal Of Electron Spectroscopy Related Phenomena 135 (2004) 167–175. https://doi.org/10.1016/j.elspec.2004.03.004.

[40] Q. Fu, T. Wagner, S. Olliges, H.-D. Carstanjen, Metal−Oxide Interfacial Reactions: Encapsulation of Pd on TiO2 (110), Journal Of Physical Chemistry B 109 (2005) 944–951. https://doi.org/10.1021/jp046091u.

[41] T. Pu, W. Zhang, M. Zhu, Engineering Heterogeneous Catalysis with Strong Metal–Support Interactions: Characterization, Theory and Manipulation, Angewandte Chemie International Edition 62 (2023) e202212278. https://doi.org/10.1002/anie.202212278.

[42] D.A. Panayotov, S.P. Burrows, J.T.Jr. Yates, J.R. Morris, Mechanistic Studies of Hydrogen Dissociation and Spillover on Au/TiO2: IR Spectroscopy of Coadsorbed CO and H-Donated Electrons, Journal Of Physical Chemistry C 115 (2011) 22400–22408. https://doi.org/10.1021/jp2065024.

[43] A. Mahdavi-Shakib, L.C. Rich, T.N. Whittaker, B.D. Chandler, Hydrogen Adsorption at the Au/TiO2 Interface: Quantitative Determination and Spectroscopic Signature of the Reactive Interface Hydroxyl Groups at the Active Site, ACS Catalysis 11 (2021) 15194–15202. https://doi.org/10.1021/acscatal.1c04419.

[44] P.A. Kots, T. Xie, B.C. Vance, C.M. Quinn, M.D. de Mello, J.A. Boscoboinik, C. Wang, P. Kumar, E.A. Stach, N.S. Marinkovic, L. Ma, S.N. Ehrlich, D.G. Vlachos, Electronic modulation of metal-support interactions improves polypropylene hydrogenolysis over ruthenium catalysts, Nature Communications 13 (2022) 5186. https://doi.org/10.1038/s41467-022-32934-5.

[45] H. Liu, Y. Wang, J.M. Bowman, Quantum Local Monomer IR Spectrum of Liquid D_2O at 300 K from 0 to 4000 cm^{-1} Is in Near-Quantitative Agreement with Experiment, Journal Of Physical Chemistry B 120 (2016) 2824–2828. https://doi.org/10.1021/acs.jpcb.6b01722.

[46] H. Belhadj, A. Hakki, P.K. J. Robertson, D. W. Bahnemann, In situ ATR-FTIR study of H 2 O and D 2 O adsorption on TiO 2 under UV irradiation, Physical Chemistry Chemical Physics 17 (2015) 22940–22946. https://doi.org/10.1039/C5CP03947A.

[47] R. Stach, P. Krebs, F. Jones, B. Mizaikoff, Observing non-classical crystallisation processes in gypsum via infrared attenuated total reflectance spectroscopy, CrystEngComm 19 (2017) 14–17. https://doi.org/10.1039/C6CE01787H.